Ocean Dynamics (2019) 69:899–911
https://doi.org/10.1007/s10236-019-01284-0

What controls the extreme flow through the Kerama Gap: a global HYbrid Coordinate Ocean Model reanalysis point of view

Zhitao Yu[1] · Edward J. Metzger[1] · Harley E. Hurlburt[2] · Ole Martin Smedstad[3]

Received: 2 August 2018 / Accepted: 17 June 2019 / Published online: 28 June 2019

Abstract
The temporal variability of volume transport from the North Pacific Ocean to the East China Sea (ECS) through the Kerama Gap (between Okinawa Island and Miyakojima Island—a part of Ryukyu Island Arc) is investigated using a 20-year global HYbrid Coordinate Ocean Model reanalysis with the Navy Coupled Ocean Data Assimilation from 1993 to 2012. We study the causes of extreme flow events defined as the volume transport through the Kerama Gap exceeding one standard deviation (4.50 Sv) above (inflow, from the North Pacific into the ECS) or below (outflow, from the ECS to the North Pacific) the mean volume transport (1.95 Sv). In our results, the impinging mesoscale eddies from the Pacific Ocean are the most important factor in controlling the extreme flow occurrence, explaining 70% (68%) of the mean extreme inflow (outflow)-mean volume transport anomaly. Extreme inflow (outflow) through the Kerama Gap is associated with the impinging anticyclonic (cyclonic) eddies along the eastern side of Okinawa and/or cyclonic (anticyclonic) eddies to the southwest of the gap. The Kuroshio frontal meanders cause the mean Kuroshio axis to shift away from (toward) the Kerama Gap during the extreme inflow (outflow)-mean events and play a secondary role in determining the extreme flow occurrence, representing 15% (14%) of the mean extreme inflow (outflow)-mean volume transport anomaly. The interannual variability of the flow through the gap also plays a subsidiary role, explaining another 13% (14%) of the mean extreme inflow (outflow)-mean volume transport anomaly.

Keywords Kerama gap · Extreme flow · Mesoscale eddy · HYCOM reanalysis · East China Sea

1 Introduction

The East China Sea (ECS) is separated from the surrounding North Pacific Ocean by the Ryukyu Island Arc along its eastern boundary. The water exchange between the ECS and the North Pacific is through channels penetrating the arc between Taiwan and Kyushu, Japan. The Kuroshio carries warm and saline water poleward (Oka and Kawabe 1998), entering and exiting the ECS through two of these channels: the East Taiwan Channel and Tokara Strait, respectively. However, the deepest channel connecting the ECS to the surrounding North Pacific is the Kerama Gap. It is located near the midpoint of the Ryukyu Island Arc between Miyakojima and Okinawa (Fig. 1) with a width of 50 km and a sill depth of 1050 m (Choi et al. 2002). The Ryukyu Current flows on the seaward side of the Ryukyu Island Arc (Ichikawa et al. 2004; Zhu et al. 2004; Thoppil et al. 2016). The Kerama Gap has been suggested as a key region for interaction between the ECS-Kuroshio and the Ryukyu Current (Nitani 1972; Andres et al. 2008a, 2008b; Jin et al. 2010; Zhou et al. 2017a, 2017b) and thus has been the subject of significant research.

Nitani (1972) suggested that water might flow into the ECS through the Kerama Gap. Previously, flow through the Kerama Gap had been observed only sparsely. Analyzing moored current meter (CM) observations, Yuan et al. (1994) reported a 5.8 Sv outflow (from the ECS to the North Pacific) through the Kerama Gap during fall 1991, but Yuan et al. (1995) estimated a 2.4 Sv inflow (from the North Pacific into the ECS) from November 1991 to September 1992. Morinaga et al. (1998) estimated a 7.2 Sv inflow through the Kerama Gap from their CM observations during 2 months from July to September 1992. Due to the relatively short observational periods, it is

Responsible Editor: Pierre De Mey-Frémaux

✉ Zhitao Yu
zhitao.yu@nrlssc.navy.mil

[1] Oceanography Division, Naval Research Laboratory, Stennis Space Center, Hancock County, MS 39529, USA

[2] Florida State University, Tallahassee, FL, USA

[3] Perspecta, Stennis Space Center, Hancock County, MS, USA

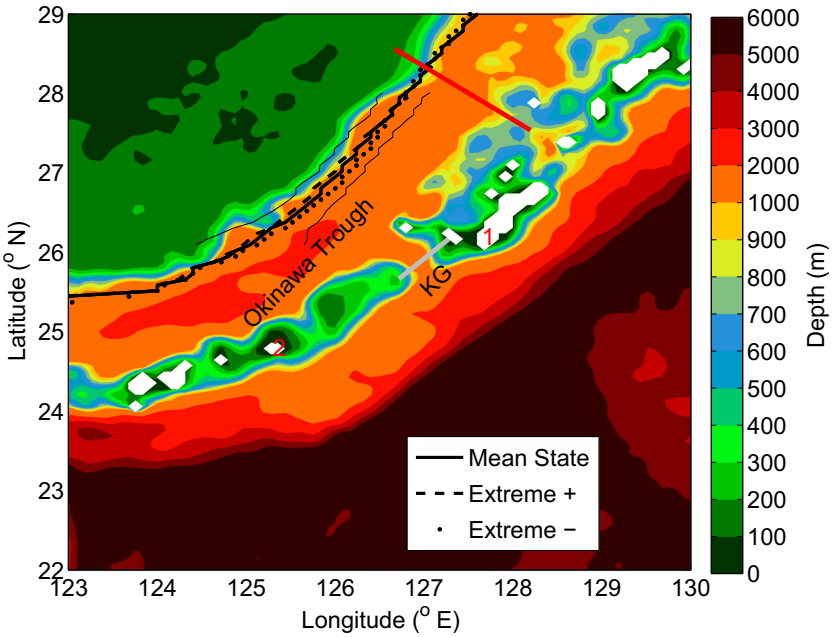

Fig. 1 Topography (meters) along the Ryukyu Island Arc near the Kerama Gap (marked KG) and the averaged location of the Kuroshio axis, defined as the location where the maximum surface velocity occurs. Heavy and thin black solid lines, respectively, represent the 20-year mean HYCOM reanalysis Kuroshio axis and its standard deviation near the Kerama Gap; black dashed line shows the average location of the Kuroshio axis during the extreme inflow-mean period; black dotted line depicts the average location of the Kuroshio axis during the extreme outflow-mean period. Okinawa (1) and Miyakojima (2) are labeled. The gray solid line represents the HYCOM transect used to determine transport through the Kerama Gap. The red line represents the PN line. White represents model land points. The land-sea boundary is defined by the 10 cm isobath, but all depths less than 5 m are set to 5 m

hard to even define the direction of the mean flow from these previous observations. The annual mean volume transport through the Kerama Gap remained uncertain until Na et al. (2014) reported a 2.0 Sv mean flow into the ECS based on 2 years of observations covering June 2009 to June 2011. The standard deviation is 3.2 Sv, which is much larger than the 2-year mean inflow and reflects large temporal variability.

Previous studies (Ichikawa 2001; Zheng et al. 2008; Andres et al. 2008a, 2008b) find that flow through the Kerama Gap generates variation of the downstream Kuroshio volume transport at the PN line (Fig. 1, red line) and Tokara Strait. The intrusion of Pacific water through the gap also modifies the Kuroshio water properties (Yu et al. 1993; Nagano et al. 2009; Nakamura et al. 2013; Zhou et al. 2017b). Dynamically, the large standard deviation of the volume transport is more important than the mean volume transport through the Kerama Gap because the 2.0 Sv mean volume transport only represents ~ 10% of the Kuroshio mean volume transport, while the 3.2 Sv standard deviation is similar to the reported 4.0 Sv standard deviation of Kuroshio volume transport through the PN line (Andres et al. 2008b) downstream of the Kerama Gap. Thus, it is important to fully understand what causes the large temporal flow variation, especially the extreme flow events with the daily volume transport exceeding one standard deviation above or below the mean transport (defined as high/low total in Na et al. 2014) through the Kerama Gap.

Observations have shown that the effects of mesoscale eddies from the interior Pacific Ocean can be transmitted via the Kerama Gap into the ECS to cause downstream Kuroshio transport variation at the PN line (Andres et al. 2008a, 2008b) and Tokara Strait (Ichikawa 2001). Na et al. (2014) also find that the temporal variability of volume transport through the Kerama Gap is related to the impinging mesoscale eddies. Andres and Cenedese (2013) further found laboratory support for this mechanism. Jin et al. (2010), on the other hand, argue that the shifting of the mean Kuroshio axis is a dominant factor in determining flow variability through the Kerama Gap by applying the self-organizing map technique to the ocean general circulation model output from the Earth Simulator.

Yu et al. (2015) demonstrated a good comparison between the observed volume transport (Na et al. 2014) through the Kerama Gap and model transport derived from a 20-year (1993–2012) global HYbrid Coordinate Ocean Model (HYCOM) reanalysis using the Navy Coupled Ocean Data Assimilation. Here we use the same global HYCOM reanalysis output to study the extreme flow through the Kerama Gap. We study the two mechanisms mentioned above (mesoscale eddies and the shifting of the mean Kuroshio axis) to determine which one controls the extreme flow through the Kerama Gap. This paper is organized as follows: the numerical model used in this study is described in Section 2. Results are presented in Section 3, followed by conclusions and discussion in Section 4.

2 Numerical model

HYCOM is a primitive equation ocean general circulation model that has been applied to large-scale, marginal sea, and coastal studies. A detailed description of HYCOM physics can be found in Bleck (2002). Below, HYCOM is briefly presented with emphasis on the model aspects that are relevant for this study.

HYCOM solves five prognostic equations: two for horizontal velocity components, a mass continuity equation, and two conservative equations that govern temperature and salinity. The prognostic equations are time-integrated using a split-explicit treatment of barotropic and baroclinic modes. In the vertical, there are three coordinate systems coexisting in HYCOM: z-coordinates in unstratified water, sigma coordinates in shallow depths, and isopycnal coordinates in the stratified ocean. Hence, HYCOM maintains the significant advantages of an isopycnal model in stratified ocean, but allows coordinate surfaces to locally deviate from isopycnals to provide more vertical resolution near the surface and in shallow coastal regions in order to better represent the upper ocean physics (Chassignet et al. 2003). With this unique feature, HYCOM serves as a good tool for simulating the circulation near the Kerama Gap, which has complex topography that covers the shallow water near the Kerama Gap and Okinawa Island, the Okinawa Trough, the continental slope, and the deep ocean.

The data assimilation technique employed for the reanalysis is a three-dimensional variational scheme (3DVAR) used within the Navy Coupled Ocean Data Assimilation (NCODA) (Cummings 2005; Cummings and Smedstad 2013). The ocean data sets assimilated by the NCODA include remotely sensed sea surface temperature (SST), sea surface height (SSH), and sea ice concentration, plus in situ surface and subsurface observations of temperature and salinity from profiles (Argo, XBTs, CTDs), ships, and moored and drifting buoys. An important component within the NCODA is forming 3D synthetic profiles from the 2D SSH and SST and statistics of the historical hydrographic database, since there are only very limited contemporaneous subsurface profile data to constrain the system. In the global HYCOM reanalysis, HYCOM assimilates synthetic temperature profiles computed using the Modular Ocean Data Assimilation System (MODAS), which models the time-averaged covariability of SSH and subsurface temperature at a given location (Fox et al. 2002). Salinity is then estimated from the synthetic temperature profiles using temperature-salinity regression relationships derived from the historical profiles archived in the MODAS database. These synthetic profiles are typically assimilated along satellite altimeter tracks, when the change in SSH from the previous analysis exceeds 3 cm.

Global HYCOM is eddy resolving with an equatorial horizontal resolution of 0.08° (1/12.5°). There are 32 hybrid coordinate layers in the vertical with potential density referenced to 2000 m, the same as the US Navy Global Ocean Forecast System (GOFS) 3.0 (Metzger et al. 2014), that has recently been replaced by 41-layer GOFS 3.1. The surface wind and thermal forcing are the 0.3125° 1-hourly Climate Forecast System Reanalysis (CFSR) products provided by the National Centers for Environmental Prediction (NCEP) (Saha et al. 2010). The ocean reanalysis was initialized from a non-assimilative global HYCOM simulation spun-up to statistical equilibrium using a climatology of the NCEP CFSR forcing. The data assimilation began on October 1, 1992, and the mesoscale eddy field adjusted to the satellite altimeter data within the first month. We analyzed model output over the period January 1993 through December 2012. The reanalysis realistically reproduces salient features of the Kuroshio, the observed Ryukyu Current velocity structure, and mesoscale eddies (Figs. 11 and 12 in Thoppil et al. 2016). The daily HYCOM output used in this study includes volume transport time series calculated through the Kerama Gap transect and velocity calculated in the ECS to identify the axis of the Kuroshio, SST, and SSH.

3 Results

The HYCOM Kerama Gap transect (Fig. 1, gray line) starts from a grid point on the ridge line to the southwest of the Kerama Gap and covers a distance of ~ 80 km, forming a 45° angle with respect to due east. Volume transport through a zonal (meridional) HYCOM transect is calculated as the product of the meridional (zonal) depth integrated barotropic velocity and the transect length. Volume transport through a diagonal HYCOM transect is estimated as a sum of the transport through the zonal and meridional transects, which starts from either end of the diagonal transect and ends where the two transects intersect.

The 20-year reanalysis mean volume transport through the Kerama Gap is 1.95 Sv, flowing into the ECS from the North Pacific Ocean, similar to Na et al. (2014) (2.0 Sv). The volume transport anomaly is calculated by removing the 20-year mean volume transport from the daily volume transport time series and is shown in Fig. 2 (thin black line). The range of the volume transport is almost 30 Sv. The standard deviation of the volume transport is 4.50 Sv, which is more than double the mean volume transport and slightly higher than that in Yu et al. 2015 (4.0 Sv) due to a longer Kerama Gap transect. The uncertainty estimate of the 20-year mean volume transport through the Kerama Gap is ± 0.28 Sv based on the auto-covariance function (Dewar and Bane 1985) of the volume transport time series.

To determine the relationship among transport components with different time periods, the daily volume transport time series is analyzed using the Morlet wavelet transform,

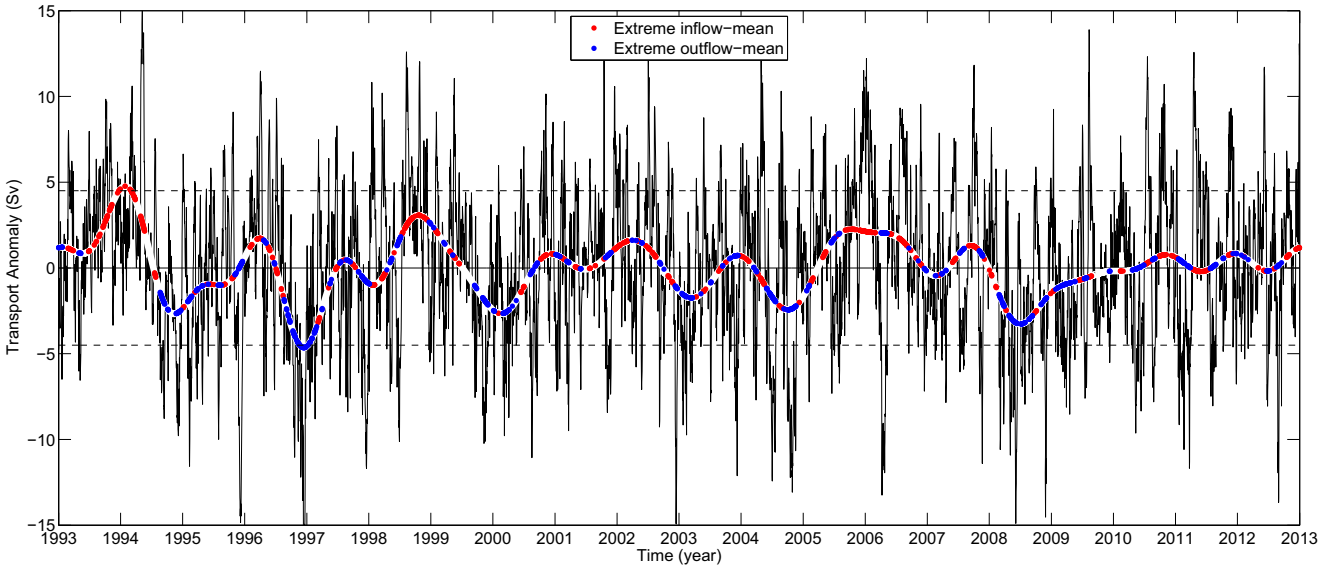

Fig. 2 Time series of the daily volume transport anomaly (Sv, with respect to the 20-year mean, thin black line) and the interannual (> 400 days) volume transport anomaly (heavy white line) through the Kerama Gap from the global HYCOM reanalysis over the period 1993 to 2012. Dashed horizontal black lines represent one standard deviation (4.50 Sv) above and below zero. The red (blue) dots represent the values of interannual volume transport anomaly at times when extreme inflow (outflow)-mean events occur. Tick marks denote the beginnings of designated years

$e^{i\omega_0\eta}e^{-\eta^2/2}$, where $\omega_0 = 6$, to satisfy the admissibility condition (Farge 1992) and is the non-dimensional frequency, and η ($\eta = t/s$, where t is time and s is the scale) is a non-dimensional "time" parameter (Torrence and Compo 1998). The transform and significance tests are performed according to the method described by Torrence and Compo (1998). The global wavelet spectrum (GWS) is calculated as the time average of all of the local wavelet spectra, which provides an unbiased and consistent estimation of the true power spectrum of a time series (Percival 1995). The wavelet power spectrum, normalized by GWS, is shown in Fig. 3. Signals with all kinds of time periods, from frontal meanders (< 30 days) to interannual (> 400 days) components, fill the wavelet spectrum. The local power spectrum exceeds the 95% confidence level for a red-noise process (black contours in Fig. 3) only with periods less than 320 days. The duration of local power spectra of high-frequency components is usually short. For components with time periods longer than 30 days, the duration varies from months to years.

It is clear from the wavelet power spectrum that the time interval of the impinging mesoscale eddies from the interior ocean varies from weeks to more than 10 months. We divide the transport time series into four period bands: interannual (> 400 days), annual (345–400 days), mesoscale eddy (30–345 days), and Kuroshio frontal meander (< 30 days) variation components (as done in Yu et al. 2015). Time series of each component are calculated, respectively, by applying a low-pass (interannual), band-pass (annual and mesoscale), and high-pass (frontal meander) filter to the time series of transport anomaly (Fig. 2, black line) depending on their frequency bands.

As mentioned in Section 1, we define "extreme inflow" and "extreme outflow" events to examine processes responsible for the large temporal transport variability through the Kerama Gap. These extreme events represent volume transport anomaly greater than 4.50 Sv ("extreme inflow-mean," defined as extreme inflow from the 20-year mean, red dots in Fig. 2), or less than − 4.50 Sv ("extreme outflow-mean," blue dots in Fig. 2). Each event (black in Fig. 4) is defined when extreme flow occurs in consecutive days or only 1 day. The number of consecutive days of each event is the duration of the extreme event (black bar in Fig. 4b, d). The maximum (minimum) transport anomaly in each extreme inflow (outflow)-mean event is taken as the transport anomaly of the event (black dots in Fig. 4), and the date when the maximum (minimum) transport occurs in each extreme inflow (outflow)-mean event is defined as the time of the extreme event.

There are 220 (223) extreme inflow (outflow)-mean events during the 20-year period (red and blue dots in Fig. 2, black in Fig. 4). These events cover 1142 (1139) extreme inflow (outflow)-mean days, which each represents 15.6% of the total 20-year period. The average extreme inflow (outflow)-mean volume transport anomaly is 6.86 (− 6.95) Sv (Table 1).

The mean duration of the extreme inflow (outflow)-mean events is 5.2 (5.1) days with a standard deviation of 5.8 (6.0) days. Short-lived extreme events occur the most. There are 170 (174) extreme inflow (outflow)-mean events that have a duration less than or equal to 6 days (Fig. 5). These short-lived events represent 77% and 78% of the extreme inflow-mean and outflow-mean events, respectively. Single-day events

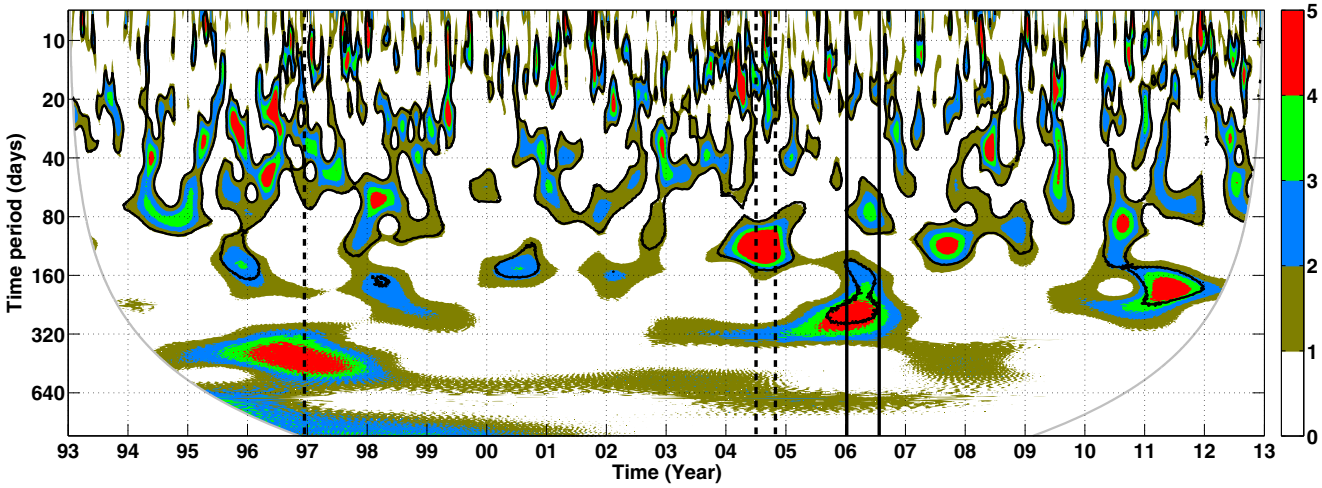

Fig. 3 Wavelet power spectrum using the Morlet wavelet normalized by the global wavelet spectrum. Colored contours are at normalized levels of 1 to 5. The black contours enclose regions of greater than 95% confidence for a red-noise process (lag-1 autocorrelation, $\propto = 0.72$). The thick gray line marks the cone of influence where edge effects become important. The thick vertical black solid (dashed) lines indicate the occurrence of extreme inflow (outflow)-mean events that last more than 30 days. Tick marks denote the beginnings of designated years

occur most frequently as 51 (59) extreme inflow (outflow)-mean events have a duration of 1 day. Long-lived extreme events are very rare with only two (three) extreme inflow (outflow)-mean events lasting more than 30 days, and the occurrence of these extreme inflow (outflow)-mean events is shown in Fig. 3 with black vertical solid (dashed) lines.

3.1 Mesoscale eddies associated with extreme flow

We first study the mean SSH anomaly (SSHA) during the extreme inflow/outflow-mean events. SSHA is defined as the SSH departure relative to the 20-year mean SSH field. Cummings and Smedstad (2013) have verified that the

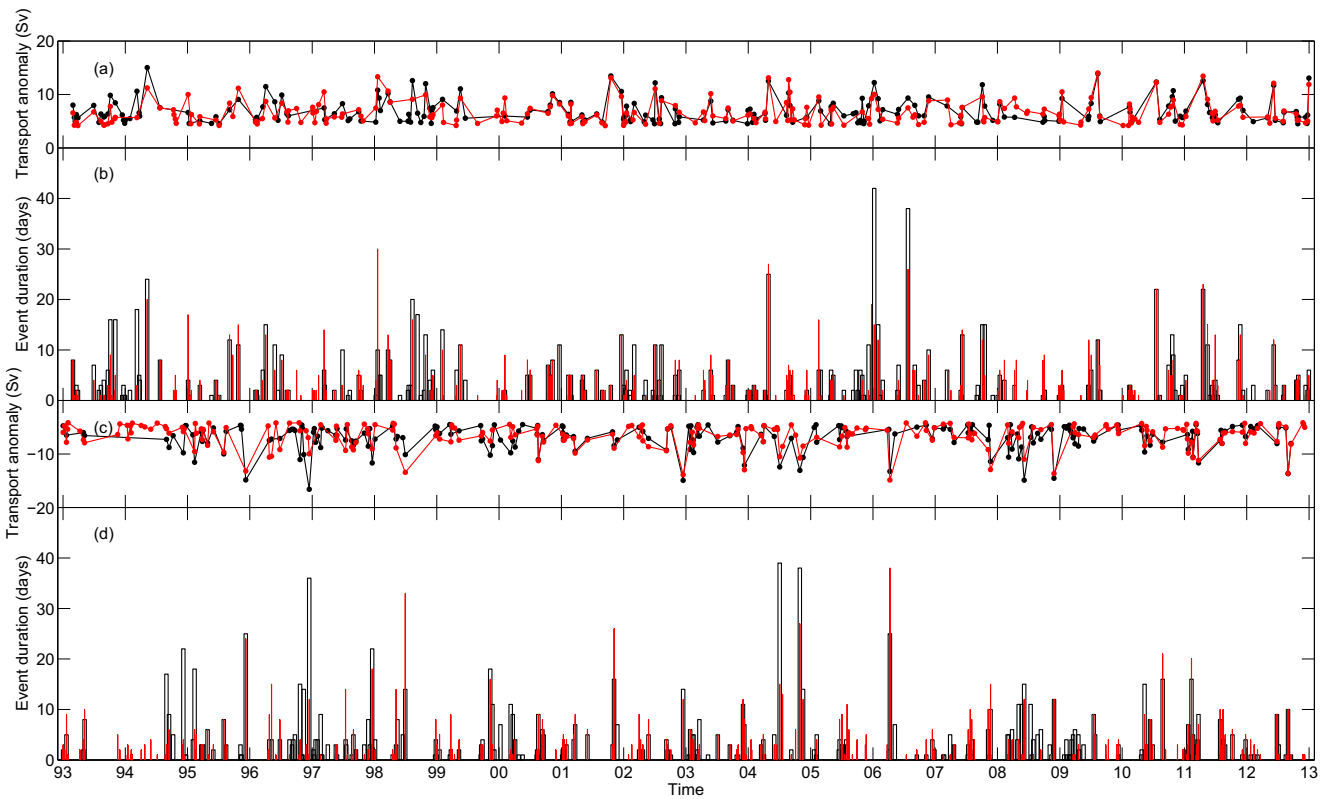

Fig. 4 Volume transport anomaly (Sv) (**a**, **c**) and duration (days) (**b**, **d**) of extreme inflow-mean events (black in **a** and **b**), extreme outflow-mean events (black in **c** and **d**), extreme inflow-interannual events (red in **a** and **b**), and extreme outflow-interannual events (red in **c** and **d**). Tick marks denote the beginnings of designated years

Table 1 Mean volume transport anomaly (Sv) through the Kerama Gap in the global HYCOM reanalysis from 1993 to 2012 for extreme flow-mean events and the corresponding contribution from the interannual variation, annual variation, mesoscale eddy component, and the frontal meander component. The contribution of the annual variation component is the difference between the total and the sum of the three other components

Mean anomaly (Sv)	Total	Interannual	Annual	Eddy	Frontal meander
Extreme inflow	6.86	0.87	0.10	4.86	1.03
Extreme outflow	− 6.95	− 0.96	− 0.20	− 4.82	− 0.97

assimilated SSH field in the Kuroshio region shows good agreement with independent infrared frontal analyses performed by the Naval Oceanographic Office. Thus, we treat the assimilated SSH as the true state. Daily SSHA on every day of the extreme inflow/outflow-mean events is averaged to represent the mean SSHA associated with extreme inflow/outflow-mean events. The most important feature revealed by the mean SSHA is a dipole formed with a pair of counter-rotating eddies centered to the east of Okinawa and southwest of the Kerama Gap (Fig. 6). Please note that both eddies straddle part of the Ryukyu Island Arc to form an elongated eddy through interaction with the islands. The spatial patterns of mean SSHA associated with the extreme inflow-mean and outflow-mean events are very similar, with a significant − 0.95 correlation coefficient (for the region shown in Fig. 6). This indicates that the two classes of eddies alter the extreme flow through the Kerama Gap in a very similar way.

Please note that the dipole is the result of the time averaging of all the extreme events over the 20-year period, mainly the impinging mesoscale eddies as can be seen later in Figs. 7, 8, 11, and 12, and a dipole eddy pair is not required to generate an extreme event. Figure 7 a shows that there is only the cyclonic mesoscale eddy to the southwest of the Kerama Gap to cause the extreme inflow on Jan. 8, 2006, while Fig. 7 b illustrates that a dipole eddy pair generates the extreme outflow through the gap on July 2, 2004. The mesoscale eddies typically propagate into this region from Pacific interior (Andres et al., 2008a, b; Na et al. 2014) as part of the return flow of the Kuroshio's non-linear recirculation gyre. The dipole is formed with an anticyclonic (cyclonic) eddy to the east of Okinawa and a cyclonic (anticyclonic) eddy to the southwest of the Kerama Gap during the extreme inflow (outflow)-mean events and is a summary of what has been observed previously (Andres et al. 2008a; Na et al. 2014). Depending on the mesoscale eddy location, the same rotational class of mesoscale eddy can increase or decrease the volume transport through the Kerama Gap. Andres et al. (2008a) demonstrate that positive transport anomalies through the Kerama Gap are associated with the impinging anticyclonic mesoscale eddies along the eastern side of Okinawa, while negative transport anomalies are associated with the impinging mesoscale cyclonic eddies. Na et al. (2014) observe that impinging cyclonic (anticyclonic) mesoscale eddies increase (decrease) volume transport through the Kerama Gap, when these mesoscale eddies are located to the south of the gap. Sometimes the same eddy propagates from the southwest of the Kerama Gap to the eastern side of Okinawa, inducing both extreme flows. But most of the time, that is not the case.

The SSH difference (SSHD) across the Kuroshio has been used as a proxy for the Kuroshio volume transport (Kawabe 1988; Andres et al. 2008b). Na et al. (2014) show that Kerama

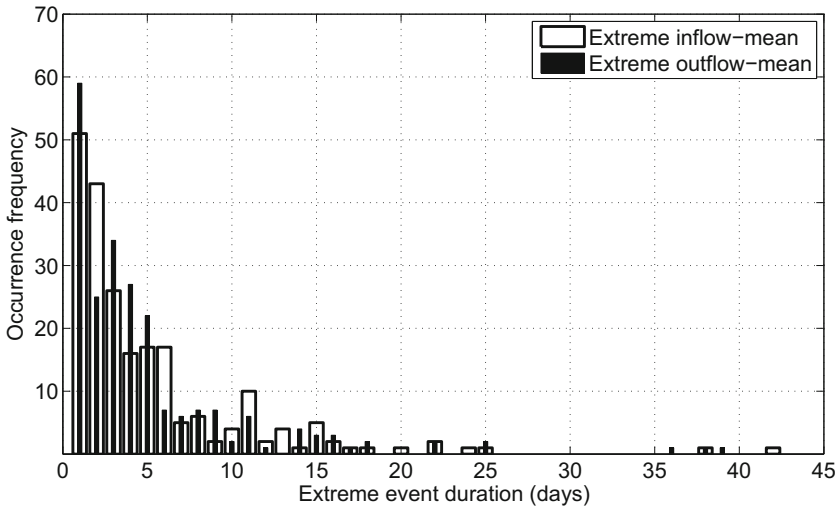

Fig. 5 Frequency of occurrence diagrams of the extreme Kerama Gap inflow-mean (open bar) and outflow-mean (solid bar) events during 1993–2012

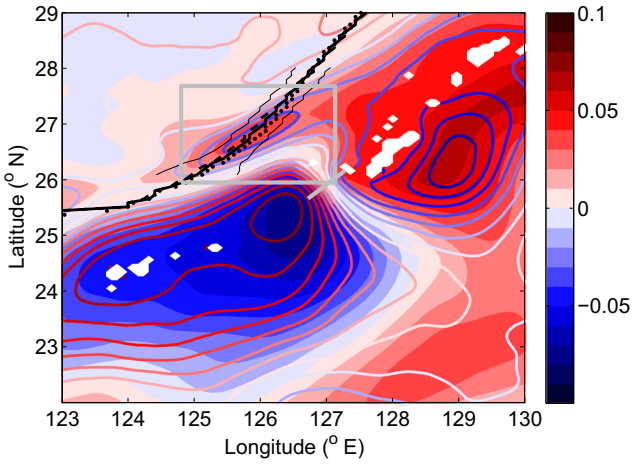

Fig. 6 Spatial pattern of the mean SSHA (m) during the extreme inflow-mean (color fill) and outflow-mean (contours) events through the Kerama Gap. The Kuroshio axes are the same as those in Fig. 1. The gray box is to show where the inner ECS eddy locates. The contour interval for both the filled colors and line colors is 1 cm

Gap transport is also well correlated with the SSHD across the gap. The correlation coefficient between the daily SSHD across the HYCOM Kerama Gap transect and the volume transport through the Kerama Gap is 0.83 over the 20-year reanalysis period. The high correlation coefficient leads us to regress volume transport anomaly onto the SSHD anomaly across the Kerama Gap transect and provides us with a regression coefficient of 0.46 Sv/cm.

The mean SSHA difference (Fig. 6) across the HYCOM Kerama Gap transect is 10.49 (− 10.28) cm during the extreme inflow (outflow)-mean events. This is equivalent to a volume transport anomaly of 4.83 (− 4.73) Sv, which represents 70% (68%) of the calculated mean extreme inflow (outflow)-mean volume transport anomaly. This suggests that the impinging mesoscale eddies are the primary cause of the extreme flow events through the Kerama Gap.

The contribution of the mesoscale eddies to the extreme inflow (outflow)-mean transport anomaly is also extracted from the time series of the mesoscale eddy components for each extreme event. The average contribution of the mesoscale eddy components to the total extreme inflow (outflow)-mean events is 4.86 (− 4.82) Sv (Table 1). These values

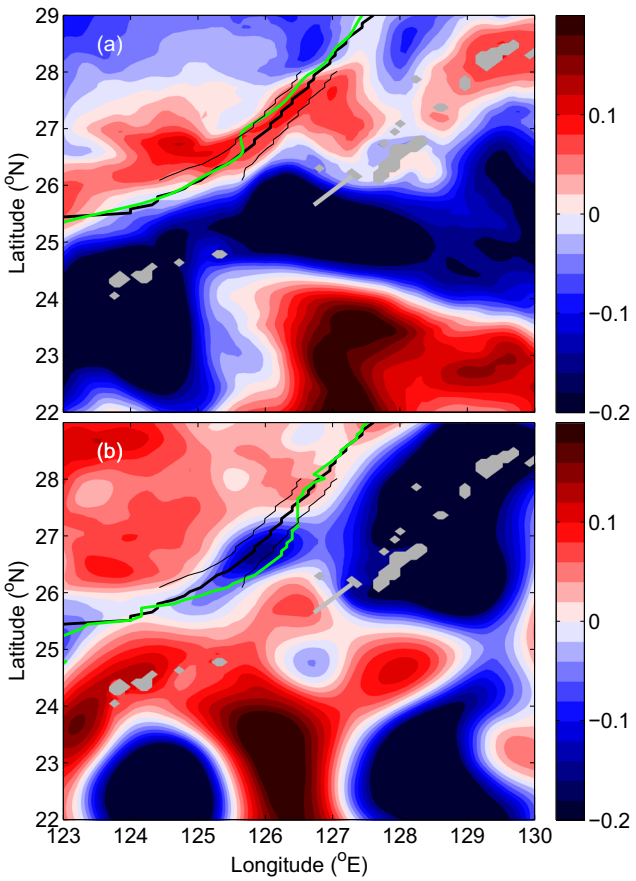

Fig. 7 Spatial pattern of the SSHA (m) and the daily Kuroshio axis (green line) during the longest extreme inflow-mean event (**a**) on Jan. 8, 2006, and outflow-mean event (**b**) on July 2, 2004, through the Kerama Gap. The mean Kuroshio axis and its standard deviation are the same as those in Fig. 1

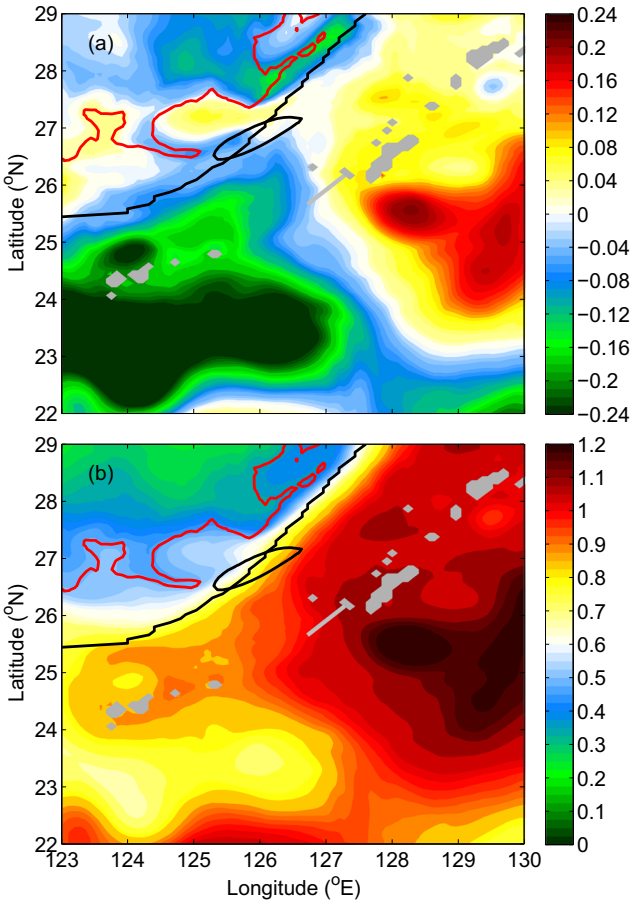

Fig. 8 Spatial pattern of **a** SSHA (m) and **b** SSH (m) on April 1, 1993. The red line is the 20 °C isotherm and represents the Kuroshio frontal meander. The black ellipse is the inner ECS eddy defined by the closed contour of the 3 mean SSHA contour associated with extreme inflow-mean events (Fig. 6). Also shown are the mean Kuroshio axis and Kerama Gap transect

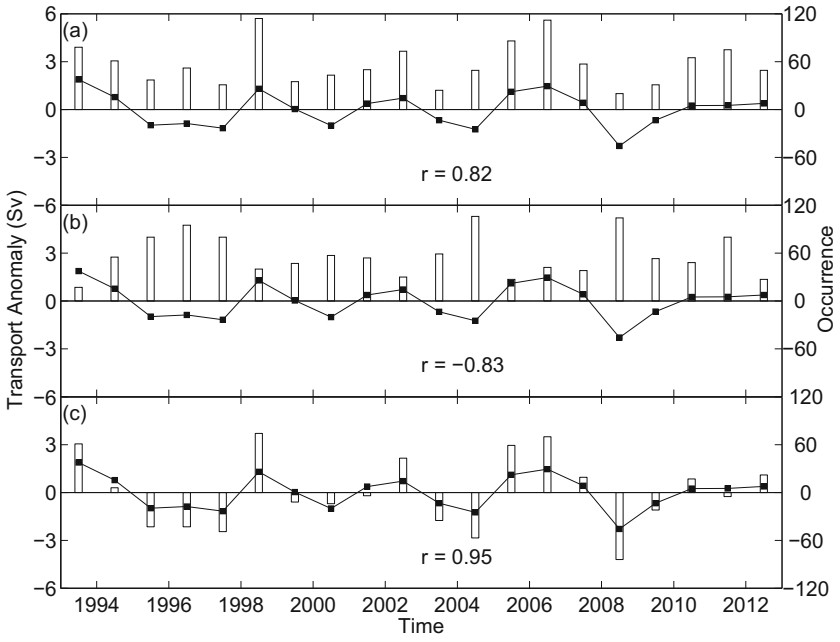

Fig. 9 Time series of yearly-averaged interannual volume transport anomaly (Sv) (black line with squares) and yearly occurrence in days (bars) of **a** extreme inflow-mean events, **b** extreme outflow-mean events, and **c** difference between extreme inflow-mean and outflow-mean events

are in good agreement with the estimates using the SSHA difference across the gap. Hence, we can use the time series of interannual, annual, and frontal meander components to calculate their corresponding contribution to the extreme events.

For non-extreme flow events, there is still a dipole pattern but with smaller eddy size and smaller SSHA (not shown). More importantly, the center of the eddies is further away from the gap than the extreme flow case. This suggests that mesoscale eddies affect the throughflow more when they get closer to the gap.

3.2 Kuroshio axis variation during extreme flow through the Kerama Gap

In this section, we demonstrate the variation of the Kuroshio axis when extreme flows occur. The Kuroshio axis is defined as the path of the maximum surface velocity in the ECS (Liu and Gan 2012). The 20-year mean Kuroshio axis (heavy black solid line in Fig. 1) shows that the main stream flows northeastward parallel to the 200 m isobath in the ECS, as mentioned by Nitani (1972). The standard deviation of the Kuroshio axis (thin black lines in Fig. 1) is approximately ±

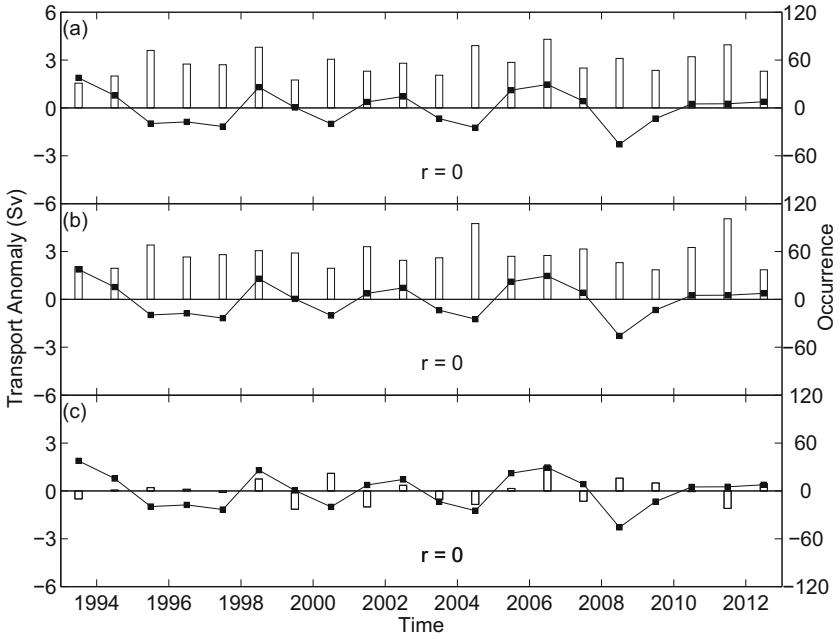

Fig. 10 Time series of yearly-averaged interannual volume transport anomaly (Sv) (black line with square) and yearly occurrence days (bars) of **a** extreme inflow-interannual events, **b** extreme outflow-interannual events, and **c** difference between extreme inflow-interannual and outflow-interannual events

0.2° perpendicular to the mean Kuroshio axis near the Kerama Gap, which agrees well with the estimate from satellite altimetry data during 1993 to 2008 by Liu and Gan (2012).

The Kuroshio axis (green line) on the day with maximum transport anomaly during the longest extreme inflow-mean and outflow-mean events is shown in Fig. 7a, b, respectively. The Kuroshio axis to the northwest of the Kerama Gap moves away from (toward) the Kerama Gap more than 1 standard deviation (thin black lines in Fig. 7) from its mean position during the extreme inflow (outflow)-mean event. The average Kuroshio axis associated with all the extreme inflow/outflow-mean events (Fig. 6, black dashed/dotted line, respectively) shows the same trend but they are less than one standard deviation of the Kuroshio axis variation.

Jin et al. (2010) find that the Kuroshio shifts away from (toward) the Kerama Gap when there is inflow (outflow) through the Kerama Gap, and our analysis shows good agreement with this finding. They found an inner ECS anticyclonic (cyclonic) circulation to the northwest of the Kerama Gap associated with inflow (outflow) through the passage. They further used this inner ECS anticyclonic (cyclonic) circulation as a proxy for the Kuroshio axis shifting away from (toward) the Kerama Gap. Mean SSHA during the extreme flow-mean events clearly shows that an inner ECS eddy (Fig. 6, in the gray box) is centered at 126.2° E and 26.8° N. The size, location, orientation, and circulation of the inner ECS eddy all agree well with what Jin et al. (2010) reported.

Jin et al. (2010) suggested that the robust high-frequency signals for each Kuroshio axis pattern is consistent with the presence of the Kuroshio frontal meanders. The Kuroshio front is defined by the isotherm that is consistent with the largest horizontal temperature gradient. Qiu et al. (1990) found that the Kuroshio front can be determined by the 20 °C isotherm during March and April. Daily SSHA and SSH fields on April 1, 1993, are shown in Fig. 8 as an example. The 20 °C isotherm (red line) clearly indicates two crests and two troughs with wavelengths of 100–200 km, in good agreement with previous research on the Kuroshio front (Sugimoto et al. 1988; Qiu et al. 1990). The Kuroshio is associated with a large cross-stream SSH gradient. The intrusion of the cold ECS water carries lower SSH toward the Kuroshio (Fig. 8b), as indicated by the cyclonic eddy following the trough entering into the inner ECS eddy area defined by the closed contour of the 3 cm mean SSHA contour associated with extreme inflow-mean events (the black ellipse, Fig. 8a). The intrusion of warm Kuroshio water into the ECS (Fig. 8b) carries higher SSH toward the ECS and generates anticyclonic eddies under the crests (Fig. 8a). Thus, the passing of the Kuroshio front crest (trough) through the inner ECS eddy region forces water to flow out (into) ECS through the Kerama Gap, presumably via horizontal advection. Similar events have been found on other days and the above is used for illustrative purposes.

This indicates that the inner ECS eddy in our analysis is also generated by the Kuroshio frontal meanders and agrees with Jin et al. (2010). And thus, the contribution of the shifting of the Kuroshio axis to the extreme flow-mean events is the same as the contribution from the Kuroshio front meanders. The average contribution from the Kuroshio frontal meander to the extreme inflow (outflow)-mean events, calculated from the time series of the frontal meander components of the volume transport through the Kerama Gap, is 1.03 (− 0.97) Sv (Table 1), which represents 15% (14%) of the calculated mean extreme inflow (outflow)-mean volume transport anomaly, smaller than the contribution from the mesoscale eddies. Jin et al. (2010) reported that the shifting of the Kuroshio axis is a dominant factor in determining flow variability through the Kerama Gap. But for the extreme flow, the shifting of the Kuroshio axis plays a secondary role in determining the extreme flow through the gap.

3.3 Interannual variability of volume transport through Kerama Gap

The 20-year volume transport time series provides an opportunity to study the impact of interannual (> 400 days) variability on the occurrence of the extreme flow-mean events. Previous studies have shown that the interannual variability of the flow through Ryukyu Island Arc is the response to the Pacific Decadal Oscillation (PDO) (Andres et al. 2009) and El Nino/Southern Oscillation (ENSO) (Kawabe 2001). The interannual variation (Fig. 2, heavy white line) can be easily identified from the volume transport anomaly time series (Fig. 2, thin black line) and the local wavelet power spectrum (Fig. 3). The magnitude of the interannual variation components (Fig. 2, heavy white line) indicates its importance to the occurrence of the extreme events. If, for example, there were no other processes involved, the interannual variation components alone would cause extreme inflow (outflow)-mean events in early 1994 (late 1996). And all five long-lived extreme events are associated with high interannual variability (Fig. 3). As mentioned in Section 3.1, we can calculate the contribution of the interannual variability to the extreme flow-mean transport anomaly from the time series of the interannual variation components (Fig. 2, heavy white line). The average contribution from the interannual variability to the extreme inflow (outflow)-mean events is 0.87 (− 0.96) Sv (Table 1), which represents 13% (14%) of the calculated mean extreme inflow (outflow)-mean volume transport anomaly.

When the interannual variability generates inflow through the Kerama Gap, it increases the possibility of extreme inflow-mean occurrence since a weaker inflow contribution from the approaching mesoscale eddies (Fig. 6, anticyclone to the east of Okinawa or/and a cyclone to the southwest of the Kerama Gap) is sufficient, and it decreases the possibility of extreme outflow-mean occurrence since a stronger outflow

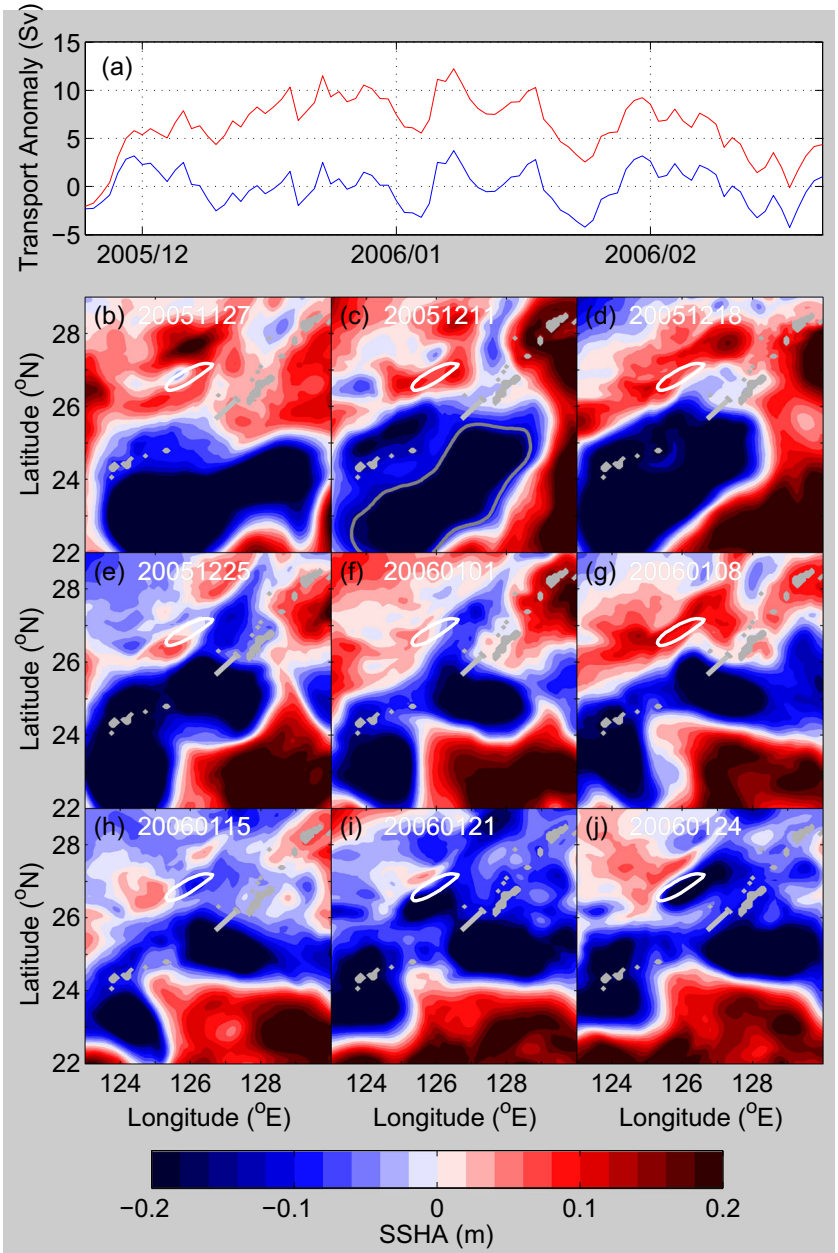

Fig. 11 **a** Time series of transport anomaly (red) and the Kuroshio frontal meander component (blue) through the Kerama Gap from November 2005 to February 2006. **b**–**j** The SSHA from nine different days during this period. The white ellipse is the inner ECS eddy defined by the closed contour of the 3 cm mean SSHA contour associated with extreme inflow-mean events (Fig. 6). The gray polygon in **c** shows the giant cyclonic eddy

contribution from the impinging mesoscale eddies (Fig. 6, a cyclone east of Okinawa or/and an anticyclone southwest of the Kerama Gap) is required to overcome the inflow contribution from interannual variability. To further determine the impact of interannual variability on extreme flow events, we calculate non-interannual transport as the transport anomaly from the interannual variation components. The standard deviation of the non-interannual volume transport is 4.18 Sv. We define the extreme flow interannual as the days during which the daily non-interannual volume transport is more/less than 4.18/− 4.18 Sv. From May 1993 to August 1994, there are strong positive interannual variations (Fig. 2). Eleven extreme outflow-interannual events (Fig. 4c, d, red) occur during this time, but no extreme outflow-mean events (Fig. 4c, d, black) during the same time period. In contrast, the interannual outflow through the Kerama Gap decreases the possibility of extreme inflow-mean occurrence and increases the possibility of extreme outflow-mean occurrence. Seven extreme inflow-interannual events (Fig. 4a, b, red) occur during October 1996 to March 1997, during which there is strong interannual outflow through the Kerama Gap (Fig. 2), but with no extreme inflow-mean events occurring at all (Fig. 4a, b, black).

Extreme inflow-mean events occur 800 (342) days, 70% (30%) of the total extreme inflow-mean occurrences during 1993–2012, when the interannual volume transport anomaly is positive (negative). The yearly occurrence days of extreme inflow-mean events (Fig. 9a, bar) and yearly averaged interannual flow anomaly (Fig. 9a, black line with square) are

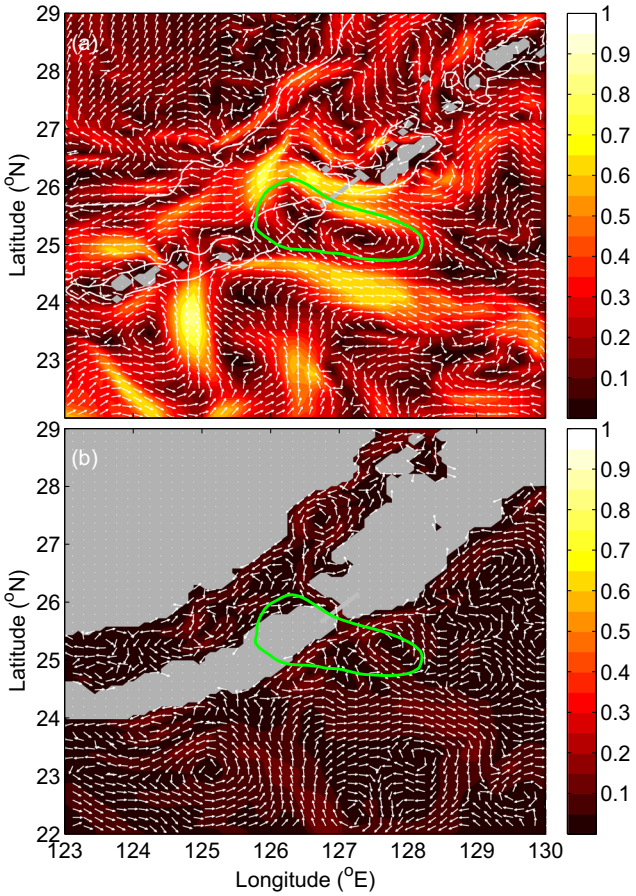

Fig. 12 Velocity anomaly (m/s) with respect to 20-year mean on January 8, 2006, at the surface (**a**) and 1000 m depth (**b**). The green polygon is the location of the cyclonic mesoscale eddy (Fig. 11g) defined by the closed contour of the − 20 cm SSHA contour associated with extreme inflow-mean events. The white line in Fig. 12a indicates the 500 m bathymetry

calculated, and the correlation coefficient is 0.82 between the two time series. Extreme outflow-mean events occur 408 (731) days, 36% (64%) of the total extreme outflow-mean days during 1993–2012, when the interannual variability causes inflow (outflow) through the Kerama Gap. The correlation coefficient is − 0.83 between yearly occurrence days of extreme outflow-mean (Fig. 9b, bar) and the yearly-averaged interannual flow anomaly (Fig. 9b, black line with square) time series.

The yearly occurrence day difference between the extreme inflow-mean and extreme outflow-mean events (Fig. 9c, bar), defined as the number of yearly extreme inflow-mean days minus the number of yearly extreme outflow-mean days, is highly correlated with the yearly-averaged interannual flow anomaly (Fig. 9c, black line with square). The correlation coefficient, 0.95, is much higher than the correlation coefficient between either the yearly occurrence days of extreme inflow mean or the extreme outflow mean and the yearly-averaged interannual volume transport anomaly. If the approaching mesoscale eddies from the Pacific interior have the same intensity and impinging frequency, the yearly occurrence difference between the extreme inflow-mean and extreme outflow-mean events should reflect the exact variation of yearly interannual volume transport anomaly. Though we are not able to make such an assumption, as shown by Hsin et al. (2013), the general conclusion is still valid, since the yearly variation of the interannual transport anomaly enhances the yearly occurrence difference between the extreme inflow-mean and outflow-mean events.

The correlation coefficients are all 0 (not significant) between yearly occurrence days of extreme inflow-interannual/outflow-interannual/occurrence difference (Fig. 10a, b, c, bar) and the yearly-averaged interannual flow anomaly (Fig. 10, black line with square) time series. This verifies that the interannual variability of the flow through the Kerama Gap plays a role in controlling the extreme flow-mean events through the passage.

4 Conclusions and discussion

Output from a 20-year global HYCOM data-assimilative reanalysis from 1993 to 2012 was used to investigate the volume transport variability through the Kerama Gap, a pathway between the North Pacific and the ECS and the deepest channel through the Ryukyu Island Arc. The 20-year mean volume transport through the Kerama Gap is 1.95 Sv into the ECS, in good agreement with observations (Na et al. 2014). The standard deviation is 4.50 Sv. We define extreme flow-mean events through the Kerama Gap as the transport exceeding one standard deviation above or below the mean volume transport and study what physical processes control the volume transport variation through this gap during the extreme flow-mean events.

Mean SSHA and Kuroshio axis variability during the extreme flow-mean events are analyzed to test two previously proposed mechanisms that affect flow variability through the Kerama Gap: (a) impinging mesoscale eddies (Andres et al. 2008a, 2008b) and (b) the shifting of the Kuroshio axis (Jin et al. 2010). Our results indicate that the impinging mesoscale eddies play the most important role, explaining 68–70% of the mean extreme volume-mean transport anomaly associated with extreme flow through the Kerama Gap. The extreme inflow (outflow)-mean event from the North Pacific (the ECS) through the Kerama Gap into the ECS (North Pacific) occurs when an anticyclone (cyclone) impinges the southeast of Okinawa or/and a cyclone (anticyclone) locates to the southwest of the Kerama Gap. The Kuroshio shifts toward (away from) the Kerama Gap during the extreme outflow (inflow) period and is closely associated with the Kuroshio frontal meanders, the same as reported by Jin et al. (2010). The Kuroshio frontal meanders play a secondary role in extreme flow through the passage, representing 15% (14%) of

the calculated mean extreme inflow (outflow)-mean volume transport anomaly.

The interannual variability of the flow through the Kerama Gap, generated by PDO and ENSO, also contributes to the occurrence of the extreme flow events. It also plays a subsidiary role, representing 13–14% of the mean extreme volume-mean transport anomaly through the gap.

4.1 The longest extreme inflow-mean event

In this section, we show an entire process of the longest extreme inflow-mean event from December 11, 2005, to January 21, 2006, to study how the mesoscale eddy affects the flow through the Kerama Gap and the cause of the frequent occurrence of the short-living events. Time series of transport anomaly through the gap from November 2005 to February 2006 are shown in Fig. 11a (red line), and the SSHA from nine different days are shown in Fig. 11b–j. The maximum inflow of this event occurs on January 8, 2006 (Fig. 11g), and the long extreme inflow-mean event is clearly dominated by the impinging cyclonic eddy.

Figure 11 b shows that the giant cyclonic eddy, marked with the gray polygon in Fig. 11c (the first day of the extreme event), was formed by merging two different cyclonic eddies on November 27, 2005. For the whole extreme event, the cyclonic mesoscale eddy exists to the south of the Kerama Gap (Fig. 11c–i). Through the interaction with Ryukyu Island Arc, the cyclonic eddy moves toward the island chain (Fig. 11d), straddles part of the island chain to form an elongated shape (Fig. 11d, e), and is separated and pushed eastward and northward by an incoming anticyclonic eddy (Fig. 11f–i).

The transport anomaly time series (Fig. 11a, red line) clearly show the high-frequency variations. These variations are dominated by Kuroshio frontal meanders (James et al. 1999) in the ECS with time periods less than 30 days. The blue line in Fig. 11a shows the frontal meander components of the transport anomaly. There are three frontal meander signals from late December 2005 to the end of January 2006 with an average time periods of 11 days, in good agreement with James et al. (1999). On January 21, 2006, the outflow generated by frontal meander (Fig. 11a) terminated the extreme flow event. All of the single-day events are generated by the frontal meanders.

The velocity anomaly on January 8, 2006, is shown in Fig. 12. The colors indicate the speed and the arrows only show the direction of the currents. The green line indicates the location of the mesoscale eddy defined by the −20 cm SSHA contour in Fig. 11g near the Kerama Gap. On the surface (Fig. 12a), the eddy-induced inflow through the Kerama Gap reaches to 0.8 m/s. Even at 1000 m deep, this cyclonic eddy still pushes water into the ECS through the gap (Fig. 12b). The surface velocity anomaly of the mesoscale eddy illustrates that two smaller mesoscale eddies in the green polygon are imbedded in a cyclonic circulation (Fig. 12a). This is due to the topography blocking. The smaller mesoscale eddy to the east of the transect is in deeper water while the other smaller mesoscale eddy is on top of the Ryukyu Island Arc with water depth less than 500 m (white line in Fig. 12a).

Acknowledgments The authors thank the anonymous reviewers for their input to improve the original manuscript. Computer time was provided by the Department of Defense (DoD) High Performance Computing Modernization Program and the simulations were performed on IBM Power 6 (daVinci) and IBM iDataPlex (Kilrain) at the Navy DoD Supercomputing Resources Center, Stennis Space Center, MS. This is NRL contribution NRL/JA/7320-18-4062. It has been approved for public release and distribution is unlimited. We wish to thank Dr. Jim Richman at Florida State University for his valuable suggestions.

Funding This effort was funded by the "6.1 Kuroshio and Ryukyu Current Dynamics" project sponsored by the Office of Naval Research under program element 0601135N. Z. Y. was supported by a Post-Doctoral Fellowship from the American Society for Engineering Education, with funding provided by the Naval Research Laboratory, Stennis Space Center, MS.

Data availability The numerical output used for this paper can be found on the http://www.hycom.org data server under the "HYCOM + NCODA Global 1/12° Reanalysis" link.

References

Andres M, Park J-H, Wimbush M, Zhu X-H, Chang K-I, Ichikawa H (2008a) Study of the Kuroshio/Ryukyu Current system based on satellite-altimeter and in situ measurements. J Oceanogr 64:937–950

Andres M, Wimbush M, Park J-H, Chang K-I, Lim B-H, Watts DR, Ichikawa H, Teague WJ (2008b) Observations of Kuroshio flow variations in the East China Sea. J Geophys Res 113:C05013. https://doi.org/10.1029/2007JC004200

Andres M, Park J-H, Wimbush M, Zhu X, Nakamura H, Kim K, Chang K-I (2009) Manifestation of the Pacific Decadal Oscillation in the Kuroshio. Geophys Res Lett 36:L16602. https://doi.org/10.1029/2009GL039216

Andres M, Cenedese C (2013) Laboratory experiments and observations of cyclonic and anticyclonic eddies impinging on an island. J Geophys Res Oceans 118:762–773. https://doi.org/10.1002/jgrc.20081

Bleck R (2002) An oceanic general circulation model framed in hybrid isopycnic-Cartesian coordinates. Ocean Model 4:55–88

Chassignet EP, Smith LT, Halliwell GR, Bleck R (2003) North Atlantic simulations with the Hybrid Coordinate Ocean Model (HYCOM): impact of the vertical coordinate choice, reference pressure, and thermobaricity. J Phys Oceanogr 33:2504–2526

Choi BH, Kim KO, Eum HM (2002) Digital bathymetric and topographic data for neighboring seas of. Korea J Korean Soc Coastal Ocean Eng 14:41–50

Cummings JA (2005) Operational multivariate ocean data assimilation. Q J R Meteorol Soc 131:3583–3604

Cummings JA, Smedstad OM (2013) Variational data assimilation for the global ocean. In: Park SK, Xu L (eds) Data assimilation for atmospheric, oceanic, and hydrologic applications, II edn. Springer-Verlag, Berlin Heidelberg. https://doi.org/10.1007/978-3-642-35088-7_13

Dewar WK, Bane JM (1985) Subsurface energetics of the Gulf Stream near the Charleston Bump. J Phys Oceanogr 15:1771–1789

Farge M (1992) Wavelet transforms and their applications to turbulence. Annu Rev Fluid Mech 24:395–457

Fox DN, Teague WJ, Barron CN, Carnes MR, Lee CM (2002) The modular ocean data assimilation system. J Atmos Ocean Technol 19:240–252

Hsin Y-C, Qiu B, Chiang T-L, Wu C-R (2013) Seasonal to interannual variations in the intensity and central position of the surface Kuroshio east of Taiwan. J Geophys Res Oceans 118:4305–4316. https://doi.org/10.1002/jgrc.20323

Ichikawa K (2001) Variation of the Kuroshio in the Tokara Strait induced by meso-scale eddies. J Oceanogr 57:55–68

Ichikawa H, Nakamura H, Nishina A, Higashi M (2004) Variability of northeastward current southeast of northern Ryukyu Islands. J Oceanogr 60:351–363

James C, Wimbush M, Ichikawa H (1999) Kuroshio meanders in the East China Sea. J Phys Oceanogr 29:259–272

Jin B, Wang G, Liu Y, and Zhang R (2010) Interaction between the East China Sea Kuroshio and the Ryukyu Current as revealed by the self-organizing map. J Geophys Res 115. doi:https://doi.org/10.1029/2010JC006437

Kawabe M (1988) Variability of Kuroshio velocity assessed from the sea-level difference between Naze and Nishinoomote. J Oceanogr Soc Jpn 44:293–304

Kawabe M (2001) Interannual variations of sea level at Nansei Islands and volume transport of the Kuroshio due to wind changes. J Oceanogr 57:189–205

Liu Z, Gan J (2012) Variability of the Kuroshio in the East China Sea derived from satellite altimetry data. Deep-Sea Res 59:25–36

Metzger EJ, Smedstad OM, Thoppil PG, Hurlburt HE, Cummings JA, Wallcraft AJ, Zamudio L, Franklin DS, Posey PG, Phelps MW, Hogan PJ, Bub FL, Dehaan CJ (2014) US Navy operational global ocean and Arctic ice prediction systems. Oceanogr. 27:32–43

Morinaga K, Nakagawa N, Osamu K, Guo B (1998) Flow pattern of the Kuroshio west of the main Okinawa Island. In: Proceedings of Japan-China Joint Symposium on Cooperative Study of Subtropical Circulation System. Seikai Natl. Fish. Res. Inst., Nagasaki, Japan, pp 203–210

Na H, Wimbush M, Park J-H, Nakamura H, Nishina A (2014) Observations of flow variability through the Kerama Gap between the East China Sea and the northwestern Pacific. J Geophys Res Oceans 119:689–703. https://doi.org/10.1002/2013JC008899

Nagano A, Ichikawa K, Ichikawa H, Konda M, Murakami K (2009) Synoptic flow structures in the confluence region of the Kuroshio and the Ryukyu Current. J Geophys Res 114. https://doi.org/10.1029/2008JC005213

Nakamura H, Nishina A, Liu Z, Tanaka F, Wimbush M, Park J-H (2013) Intermediate and deep water formation in the Okinawa Trough. J Geophys Res Oceans 118:6881–6893. https://doi.org/10.1002/2013JC009326

Nitani H (1972) Beginning of the Kuroshio. In Staommel H and Yoshida K (ed) Kuroshio. Univ. of Wash. Press, Seattle

Oka E, Kawabe M (1998) Characteristics of variations of water properties and density structure around the Kuroshio in the East China Sea. J Oceanogr 54:605–617

Percival DP (1995) On estimation of the wavelet variance. Biometrika 82: 619–631

Qiu B, Toda T, Imasato N (1990) On Kuroshio front fluctuations in the East China Sea using satellite and in situ observational data. J Geophys Res 95:18191–18204

Saha S et al (2010) The NCEP Climate Forecast System Reanalysis. Bull Amer Meteor Soc 91:1015–1057. https://doi.org/10.1175/2010BAMS3001.1

Sugimoto T, Kimura S, Miyaji K (1988) Meander of the Kuroshio front and current variability in the East China Sea. J Oceanogr Soc Jpn 44: 125–135

Thoppil P, Metzger EJ, Hurlburt HE, Smedstad OM, Ichikawa H (2016) The current system east of the Ryukyu Islands as revealed by a global ocean reanalysis. Prog Oceanogr 141:239–258. https://doi.org/10.1016/j.pocean.2015.12.013

Torrence C, Compo GP (1998) A practical guide to wavelet analysis. Bull Am Meteorol Soc 79:61–78

Yu H, Su J, Miao Y (1993) The low salinity water (LSW) core of Kuroshio in the East China Sea and intrusion of western boundary current (WBC) east of Ryukyu Islands (in Chinese). In: Essays on the investigation of Kuroshio, 5th edn. Ocean Press, Beijing, pp 225–241

Yu Z, Metzger EJ, Thoppil P, Hurlburt HE, Zamudio L, Smedstad OM, Na H, Nakamura H, Park J-H (2015) Seasonal cycle of volume transport through Kerama Gap revealed by a 20-year global Hybrid Coordinate Ocean Model reanalysis. Ocean Model 96: 203–221. https://doi.org/10.1016/j.ocemod.2015.10.012

Yuan Y, Takano K, Pan Z, Su J, Kawatate K, Imawaki S, Yu H, Chen H, Ichikawa H, Umatani S (1994) The Kuroshio in the East China Sea and the currents east of the Ryukyu Islands during autumn 1991. La Mer 32:235–244

Yuan Y, Su J, Pan Z, Chen H, Ichikawa H, Imawaki S, Kawatate K, Takano K, Umatani S-I (1995) The western boundary current east of the Ryukyu Islands. La Mer 33:1–11

Zheng XT, Liu QY, Hu HB, Miyazawa Y, Jia YL (2008) The study of temporal and spatial characteristics of western boundary current east of Ryukyu submarine ridge and the transport of Kuroshio in East China Sea (in Chinese). Acta Oceanol Sin 30:1–9

Zhou W, Yu F, Nan F (2017a) Water exchange through the Kerama Gap estimated with a 25-year Pacific HYbrid Coordinate Ocean Model. Chin J Oceanol Limnol 35:1287–1302. https://doi.org/10.1007/s00343-017-6141-2

Zhou W, Yu F, and Nan F (2017b) Water exchange via the Kerama Gap affects salinity of the Kuroshio (in Chinese). Oceanol Limnol Sin Doi:https://doi.org/10.11693/hyhz20170200038

Zhu X-H, Ichikawa H, Ichikawa K, Takeuchi K (2004) Volume transport variability southeast of Okinawa Island estimated from satellite altimeter data. J Oceanogr 60:953–962